

Superconducting Spin Valves Based on a Single Spiral Magnetic Layer

N.G. Pugach^{1,*}, M.O. Safonchik¹, V.I. Belotelov^{3,4}, T. Ziman⁵, and T. Champel⁶

¹ HSE University, Moscow 101000, Russia

² A.F. Ioffe Physical-Technical Institute, St Petersburg RU-194021, Russia

³ Lomonosov Moscow State University, Leninskie Gory 1(2), Moscow 119991, Russia

⁴ V.I. Vernadsky Crimean Federal University, Vernadsky Prospekt 4, Simferopol 295007, Crimea

⁵ Institut Laue-Langevin, BP 156, 41 avenue des Martyrs, Grenoble Cedex 9 38042, France

⁶ Université Grenoble Alpes, CNRS, LPMMC, Grenoble 38000, France



(Received 30 September 2021; revised 18 January 2022; accepted 19 September 2022; published 1 November 2022)

A detailed investigation of a superconducting spin-triplet valve is presented. This spin valve consists of a superconducting film covering a metal with an intrinsic spiral magnetic order, which could result from competing isotropic exchanges or, if the crystal lattice breaks central symmetry, from asymmetric Dzyaloshinskii-Moriya exchange. Depending on the anisotropy, such a metal may change its magnetization either from a spiral to uniform order, as seen in Ho and Er, or in the direction of the spiral itself, as in crystals of the B20-type structure [such as MnSi, (Fe,Co)Si, FeGe, etc.]. The nonuniform magnetic order controls the appearance of long-range triplet superconducting correlations at strong exchange fields, affecting the detailed character of the proximity effect. We show that the magnetic control of the spin-valve behavior can also be obtained from moderately low exchange fields (typically associated to negligible long-range triplet correlations), thanks to an orientation-dependent averaging mechanism of the magnetic inhomogeneity on the scale of the Cooper pairs. Our numerical calculations reveal that the spin-valve effect is in fact magnified at moderately low exchange fields, when the exchange splitting in the spiral magnet is comparable to the superconducting gap, and the spiral period is less than or equal to the superconducting coherence length in the magnet multiplied by 2π .

DOI: 10.1103/PhysRevApplied.18.054002

I. INTRODUCTION

Superconducting spintronics is a modern field in cryogenic nanoelectronics [1] that has emerged since the second decade of this century [2]. As in traditional spintronics, the aim is to utilize spin transfer for information processing. Since a spin current is not necessarily accompanied by a charge transfer, such devices, combining magnetic and superconducting order, promise to be energetically efficient. This field is currently in development, with the demonstration of device concepts [3–5]. Magnetic control of charge transfer is a key mechanism of spintronic devices and, in particular, of the functionality of magnetic memory (MRAM) units. Like traditional MRAM elements based on magnetic tunnel junctions and spin-transfer-torque elements, superconducting spin valves (SSVs) were proposed theoretically [6–8], and are currently at the stage of optimization [9–11].

The magnetization reversal of a ferromagnetic (F) element may provide for magnetic control of the Josephson current [12–15] or may change the superconducting critical temperature T_c both in the $F/S/F$ [16] and $S/F/F$ [17] configurations, where S denotes a superconducting film. The possibility of tuning superconductivity by the mutual orientation (parallel or antiparallel) of two F layers in this type of SSV was shown in different experiments [18–21]. The shift δT_c in the critical temperature was assumed to be due to the paramagnetic effect, i.e., the breaking of the Cooper pairs by the spin polarizations induced within the superconducting layer by the ferromagnetic layers. When the magnetizations in the F layers are antiparallel, these polarizations effectively cancel out, while in the parallel configuration the induced polarizations act cooperatively to suppress superconductivity. A shift in T_c between two different magnetic configurations opens the way to realize an optimized switch from a superconducting to a normal state. The formal value of the magnetoresistance is then infinite, since the resistance changes from zero in the superconducting state, to a finite value in the normal state.

* npugach@hse.ru

The triplet mechanism of the SSV effect was later deduced in the same structures. It was shown that a non-collinear magnetization configuration may provide an even larger shift in δT_c [9,22–24] due to the appearance of long-range triplet superconducting correlations (LRTCs) [25–28]. The production of the LRTC, which can be seen as one more channel for the draining of the Cooper pairs from the superconductor, enhances the proximity effect, and as a result reduces T_c more efficiently. A full T_c switch, where δT_c is larger than the superconducting transition width, has been reached in a few experiments [29–32]. Nevertheless, the improvement and optimization of SSVs still remain both a theoretical and experimental challenge [33–39]. Possible ways to improve the properties of SSVs include optimization of the structures, via the technology of their preparation, the quality of interfaces, and the choice of materials, including strong, half-metallic, or insulating ferromagnets.

Recently, layers of the spiral magnet (M) holmium have been used as spin mixers, improving the magnetoresistive properties of SSVs [9,40–45]. Taken separately in a S/M bilayer, a spiral or conical magnetic layer also provides a shift of T_c when an external magnetic field is applied [45,46]. Indeed, a parallel magnetization of the spiral magnetic layer suppresses the LRTC, leading to a change in T_c . However, the return to the initial helimagnetic state would require heating the sample above the Curie temperature, much higher than T_c . This would make this kind of SSV difficult to use in low-temperature electronics.

A further problem to consider, inherent both for SSVs and Josephson MRAM, is the so-called half-select problem [47]. This occurs in the conventionally known RAM scheme with two sets of crossing “word” and “bit” lines, for example, along the “ X ” and “ Y ” directions. The control signal should switch the state of a particular element at the crossing of two lines in a net, whereas the half-amplitude signal should not cause a switch of any other elements along the crossing lines. This requirement provides for an addressable switch of any particular memory element in RAM. It means that the two logical states of a memory element must be separated by a potential barrier. Multilayered structures with continuous magnetization reversals do not solve this problem. In contrast, it has been pointed out [48] that if a spiral magnet M has a potential barrier between two spiral directions due to cubic anisotropy, the resulting S/M bilayer may work both as a SSV and a Josephson MRAM. Recently, a way of controlling such SSVs was developed [49], based on magnonic relaxation after a magnetic field pulse. This method is attractive as it is nondestructive of the superconducting state. The spiral SSVs allowing such a means of control should have parameters (record-readout speed and stability) comparable with modern MRAM [49].

In this paper we explore this idea quantitatively [48] by considering spiral magnets of the B20 family, such as MnSi, (Fe,Co)Si, FeGe, in bulk, or etched films, to provide the full T_c switch by a change of the spiral direction. This is possible because the cubic noncentrosymmetric magnetic structure of the B20 crystal family [50–52] provides an asymmetric Dzyaloshinskii-Moriya exchange [53]. The magnetic spiral structure, characterized by the spiral vector \mathbf{Q} , may be aligned in a few different, but equivalent, directions under the control of a weak external magnetic field. These preferred directions are determined by the potential barriers that depend on the compound [54]. This provides the advantage previously mentioned for their use as MRAM switchable elements. Such magnetic compounds and their films are now the subject of much interest [55,56] as a medium for magnetic topological defects like skyrmions. Thin films of MnSi have a strong in-plane magnetic anisotropy and host only magnetic spiral order with the vector \mathbf{Q} perpendicular to the plane of the film [57]. The T_c in such a superconducting bilayer may be controlled via a reversible uniform magnetization of the films in an external magnetic field. Such elements may be used in biased RAM. Here we investigate theoretically the possibilities of using S/M bilayers as switchable elements for cryogenic electronics application, useful for both SSVs and MRAM. We find that the magnitude of δT_c is a nonmonotonic function of the spiral wave vector that depends on the amplitudes of the exchange field. This behavior can be exploited for the optimization of the structures.

This paper is organized as follows: Sec. II presents the model and the general method for deriving T_c in the S/M bilayer, while Sec. III discusses the numerical results we obtain for T_c . Section IV concludes this work. The details of the analytical calculations are presented in the Appendix.

II. MODEL

To describe the superconducting proximity effect with a spiral magnet, we use linearized Usadel equations in the form [58] valid close to T_c in the dirty limit, which is usually satisfied in hybrid structures prepared by sputtering. In this limit, the superconducting coherence lengths in the M and S layers are given by $\xi_{f,s} = \sqrt{D_{f,s}/2\pi T_{cb}}$, where $D_{f,s}$ are the corresponding electron diffusion coefficients and T_{cb} is the critical temperature of the bulk superconductor.

Here we develop a method of calculation that allows us to consider the limits of both weak and strong exchange splitting h , as well as to examine the behavior at arbitrary values of h (provided the Usadel equations remain valid) for spirals of both long and short periods. Moreover, we take the thickness of the magnetic layer to be finite, and include related effects, such as reentrant superconductivity, which also depends on the spiral magnetic order. The

third improvement of the current method in comparison with previous theories [48,58–64] is the determination of T_c at arbitrary angles between the spiral wave vector \mathbf{Q} and the plane of the S layer.

A. Usadel equations for the magnetic spiral inclined at an arbitrary angle α

We consider a superconducting layer (S) with a finite thickness d_s in proximity with a layer of spiral magnet (M) of thickness d_f . The spiral vector \mathbf{Q} , is taken to be inclined with an angle α with respect to the OZ direction, orthogonal to the plane of the layers, see Fig. 1. We assume that \mathbf{Q} lies in the XOZ plane, while the XOY plane coincides with the SM interface [65].

The linearized Usadel equations have the general form [58,66]

$$\begin{aligned} (D\nabla^2 - 2|\omega|)f_s &= -2\pi\Delta + 2i\operatorname{sgn}(\omega)\mathbf{h}\cdot\mathbf{f}_t, \\ (D\nabla^2 - 2|\omega|)\mathbf{f}_t &= 2i\operatorname{sgn}(\omega)\mathbf{h}f_s, \end{aligned} \quad (1)$$

where the singlet f_s and triplet $\mathbf{f}_t = (f_x, f_y, f_z)$ spin components of the anomalous Green's function describe the different superconducting correlations. The singlet superconducting order parameter $\Delta = \Delta(z)$ is nonzero only in the S layer, while the exchange spin splitting $\mathbf{h}(x, z)$, aligned along the local magnetization, is nonzero only in the M layer. The spiral vector \mathbf{Q} enters in Eq. (1) through the exchange spin splitting, which for $\alpha = 0$ reads $\mathbf{h}(\mathbf{r}) = h(\cos[Qz], \sin[Qz], 0)^T$. By taking into account the even symmetry of the singlet components and the odd symmetry of the triplet ones with respect to the Matsubara frequency $\omega \equiv \omega_n = \pi T(2n + 1)$ with n a positive or negative integer, we may consider in the following only positive ω .

As a result of the presence of the S/M interface and of the proximity effect, the superconducting correlations naturally depend on the distance to the interface, i.e., they exhibit a z dependence. For an inclined spiral vector \mathbf{Q} ,

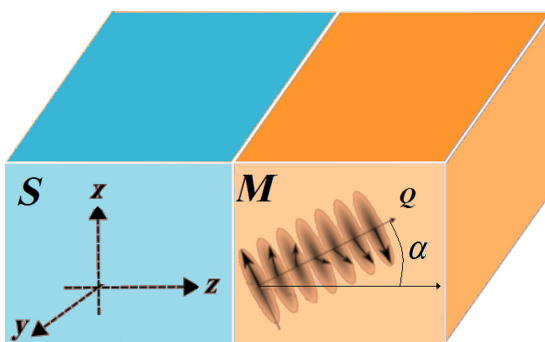


FIG. 1. Sketch of the studied SSV with the spiral wave vector \mathbf{Q} tilted at an angle α to the normal of the S/M interface.

the magnetic vector \mathbf{h} displays an explicit spatial dependence on both variables x and z , so that the problem we consider is in general a two-dimensional one. However, as we show in the Appendix, the extra dependence on x due to the rotating spiral when $\alpha \neq 0$ can be gauged away via a suitable transformation on the triplet vector \mathbf{f}_t , so that the original problem is mapped to the following effective one-dimensional one for the triplet components $f_-(z)$ and $f_+(z)$ in the magnetic layer (see the Appendix for details):

$$\begin{aligned} \left(\frac{\partial^2}{\partial z^2} - \frac{2\omega}{D_f} \right) f_s &= i \frac{h}{D_f} [f_- - f_+], \\ \left[\frac{\partial^2}{\partial z^2} \mp 2iQ \cos \alpha \frac{\partial}{\partial z} - Q^2 - \frac{2\omega}{D_f} \right] f_{\pm} &= \mp 2i \frac{h}{D_f} f_s, \end{aligned} \quad (2)$$

with h and Q the amplitudes of the exchange splitting and of the spiral wave vector, respectively. The form of these equations reproduces the limiting cases of spirals both orthogonal and parallel to the interface $\alpha = 0, \pi/2$ that were considered in Refs. [48,58]. The presence of linear terms in the spiral vector Q reflects the chirality of the spiral, which is related to the broken inversion symmetry of the magnetic lattice that can be found in compounds of the B20 family, for instance. The chirality makes the calculations rather more complicated than for the case where uniform magnetization can be assumed.

B. The characteristic equation

If the M layer is semi-infinite and occupies the half-space $z > 0$, the solutions of the linear differential Eq. (2) take the simple form $f_j(z) = u_j \exp(-k_j z)$, where $j = s, +, -$. We take the more general situation of a M layer with a finite thickness. This means that we also have to consider spatial solutions with $-k_i$, describing the waves reflected from the free M interface.

The amplitude coefficients for these solutions are determined by the boundary conditions. Here the wave vectors $\pm k_i$ are the eigenvalues of the system (2) and we represent in the following the components of these two related eigenvectors by u_j, v_j . Let us also introduce the characteristic momenta $k_\omega = \sqrt{2\omega/D_f}, k_h = \sqrt{h/D_f}$. Equation (2) leads to the system of algebraic equations

$$\begin{aligned} (k^2 - k_\omega^2)f_s - i k_h^2 f_- + i k_h^2 f_+ &= 0, \\ \pm 2i k_h^2 f_s + (k^2 - k_\omega^2 \pm 2iQk \cos \alpha - Q^2)f_{\pm} &= 0. \end{aligned} \quad (3)$$

The characteristic equation of this system yielding the eigenvalues k_i is

$$\begin{aligned} [(k^2 - k_\omega^2 - Q^2)^2 + 4Q^2 k^2 \cos^2 \alpha] (k^2 - k_\omega^2) \\ + 4k_h^4 (k^2 - k_\omega^2 - Q^2) = 0. \end{aligned} \quad (4)$$

This bicubic equation displays three pairs of solutions $\pm k_i$ with Real $k_i > 0$, which are the eigenvalues of the system

(2). In the limit $k_h^2 \gg Q^2, k_\omega^2$ the three eigenvalues are similar to those found in the orthogonal case: two short-range components $k_\pm \approx (1 \pm i)k_h$, and one long-range component $k_0 \approx \sqrt{k_\omega^2 + Q^2}$. Assuming a large exchange energy of $h = 100$ meV (it is typically of the order of 1 eV in ferromagnetic transition metals), one may estimate the quasi-momenta as [48] $k_h = \xi_h^{-1} \sim 1 \text{ nm}^{-1}, k_\omega \sim 1/7 \text{ nm}^{-1} = 0.14 \text{ nm}^{-1}$, that yields the inequalities $k_h > Q > k_\omega$. The approximation of strong exchange energy for the values of $k_{\pm,0}$ is thus valid for $h = 100$ meV with an accuracy of two decimal places. The approximate eigenvectors $(-1, -1, 1), (1, -1, 1)$, and $(0, 1, 1)$ associated with these eigenvalues have an accuracy of only one decimal place, however.

In the general case we solve the characteristic equation exactly (4), with the eigenvectors so found u_j and v_j written in the Appendix. Note that, in the approximation of large exchange splitting, the eigenvalues and eigenvectors coincide with those described previously in the two limiting cases of the spiral parallel to the S/M interface [58,67] ($\alpha = \pi/2$) and of the spiral orthogonal to the S/M interface ($\alpha = 0$) for semi-infinite [48] and finite [59] M layers.

The solution of the Usadel equations for the finite M layer may finally be found in the general form

$$f_j(z) = \sum_i A_i u_j(k_i) \exp(-k_i z) + B_i v_j(k_i) \exp(k_i z). \quad (5)$$

The coefficients A_i and B_i are then determined from the boundary conditions, as discussed in the next section.

C. Boundary conditions

Kupriyanov-Lukichev [68] boundary conditions for the singlet and triplet components of the anomalous Green's function read at the free interfaces

$$\frac{\partial}{\partial z} f_{s,t} = 0, \quad (6)$$

and at the SM interface located at $z = 0$

$$\begin{aligned} \xi_s \frac{\partial}{\partial z} f_{s,t}^S &= \gamma \xi_f \frac{\partial}{\partial z} f_{s,t}, \\ f_{s,t}^S &= f_{s,t} - \gamma_b \xi_f \frac{\partial}{\partial z} f_{s,t}. \end{aligned} \quad (7)$$

We introduce here the dimensionless interface parameters $\gamma_b = R_b A \sigma_f / \xi_f$ and $\gamma = (\sigma_f / \sigma_s)(\xi_s / \xi_f)$. The quantities R_b and A are the resistance and the area of the S/M interface, respectively, and $\sigma_{f,s}$ is the conductivity of the M or S metal. Inclusion of the superscript S in the components f_s^S or f_t^S is used to specify that the correlations are evaluated from the superconducting side, while the absence of superscript holds for the magnetic side.

Since the Usadel equations have been rewritten in terms of the transformed triplet components $f_\pm(z)$, we need to derive the boundary conditions for these functions instead. As shown in the Appendix, we find the boundary conditions for the free interfaces at $z = d_f$ and $z = -d_s$ for the inclined case corresponding to the linearized Usadel equations (2)

$$\begin{aligned} \frac{\partial}{\partial z} f_s(d_f) &= 0, & \frac{\partial}{\partial z} f_\pm(d_f) &= \pm iQ \cos \alpha f_\pm(d_f), \\ \frac{\partial}{\partial z} f_{s,\pm}^S(-d_s) &= 0, \end{aligned} \quad (8)$$

and the boundary conditions at the S/M interface at $z = 0$

$$\begin{aligned} \xi_s \frac{\partial}{\partial z} f_s^S(0) &= \gamma \xi_f \frac{\partial}{\partial z} f_s(0), \\ \xi_s \frac{\partial}{\partial z} f_\pm^S(0) &= \gamma \xi_f \left(\frac{\partial}{\partial z} \mp iQ \cos \alpha \right) f_\pm(0), \\ f_s^S(0) &= f_s(0) - \gamma_b \xi_f \frac{\partial}{\partial z} f_s(0), \\ f_\pm^S(0) &= f_\pm(0) - \gamma_b \xi_f \left(\frac{\partial}{\partial z} \mp iQ \cos \alpha \right) f_\pm(0). \end{aligned} \quad (9)$$

The sign \pm in front of the contributions depending on Q expresses the chirality of the magnetic spiral: clockwise or anticlockwise. In the presence of a finite thickness of the magnet, this chirality adds a degree of complexity that was absent in previous work. We note though that the superconducting critical temperature turns out to be independent of the sign of the chirality, owing to the spin symmetry of the superconducting wave function in S .

D. Critical temperature calculation

The singlet component $f_s^S(z)$ in the superconductor depends on the superconducting gap $\Delta(z)$, which is calculated self-consistently. The required closed boundary value problem for the singlet component f_s^S includes the Usadel Eq. (2) in the superconducting layer, and the boundary condition in the form

$$\xi_s \frac{\partial}{\partial z} f_s^S \Big|_{z=0} = -W f_s^S \Big|_{z=0}. \quad (10)$$

The real-valued quantity W contains the entire information about the proximity effect with the spiral magnet, and may be written as

$$W = \gamma \left[\frac{\sum_i S_i u_s(k_i)}{\xi_f \sum_i R_i k_i u_s(k_i)} + \gamma_b \right]^{-1}, \quad (11)$$

with the coefficients R_i and S_i defined in the Appendix.

Finally, we compute numerically the critical temperature T_c of the superconducting layer, using the self-consistent equation

$$\ln \frac{T_{cb}}{T_c} = \pi T_c \sum_{\omega=-\infty}^{\infty} \left(\frac{1}{|\omega|} - \frac{f_s^S(z)}{\pi \Delta(z)} \right) \quad (12)$$

and the method of the fundamental solution [58,69,70].

E. Model parameters

For the realization of the presently studied SSV, different types of spiral magnets may be considered, thus providing various possible ranges of values for the model parameters. This variety can naturally be exploited to optimize the switching control and the spin-valve behavior in the S/M bilayer. In this section, we address in some detail the possibilities currently available for real materials and the associated variable ranges, in particular for the magnitudes of the exchange splitting h or for the spiral wave vector Q .

Metals of the B20 family like MnSi, (Fe,Co)Si, FeGe, etc., are arranged in a crystal lattice of cubic symmetry with broken inversion symmetry. The latter provides an asymmetric Dzyaloshinskii-Moriya exchange, leading to spiral magnetic order. For Lanthanide metals like Ho or Er, the spiral magnetic order stems from the competing magnetic exchanges of nearest neighbor and next-nearest neighbors. Although the microscopic natures differ, at the level of the proximity effect these magnetic materials exhibit similar properties when described within a mean-field approximation.

Because of the lattice symmetry in B20 materials, the magnetic spiral characterized by the vector \mathbf{Q} may align in a few different directions in the ground state, in the absence of an external magnetic field. Depending on the compound, the preferred spiral directions may be along the cubic axes [100], [010], [001], as for (Fe, Co)Si and MnGe, and along the diagonals of the cube [$1 \pm 1 \pm 1$], as for MnSi. Depending on the magnetic history [54], the spiral may even have an arbitrary direction at a weak cubic anisotropy, as, for example, in (Fe, Co)Si. The direction of \mathbf{Q} may be controlled by a relatively weak external magnetic field, of the order of 100 Oe for MnSi. It is useful for the applications in SSVs to have the control field lower than the critical magnetic field of superconducting films, which is approximately 30 kOe for the in-plane direction of the Nb superconductor. Very recently, a method to control a bilayer SSV, which does not perturb its superconducting state has been proposed and optimized [49] via numerical experiments on the MnSi/Nb bilayer SSV. Switching between a few ground-state magnetic configurations with different directions of the magnetic spiral \mathbf{Q} , that are separated by potential barriers, was proposed by applying a magnetic field pulse several hundred ps in duration and

several kOe in magnitude. Such a pulse would not itself destroy the superconducting state of the Nb layer, but leads to the excitation of magnons in the magnetic layer, that then trigger the reorientation process of the magnetic spiral [49]. The system can be switched back and forth by magnetic fields of opposite signs along a single direction of the plane of the layers. This allows for easy control. The switching time is estimated [49] to be several nanoseconds, which coincides with the scales of the spin-transfer-torque MRAM recording time, making this method attractive for energy-saving cryogenic electronics.

The absolute value of the spiral vector is defined as $Q = 2\pi/\lambda$, where λ is the spiral spatial period. The spiral antiferromagnets of the B20 family may have short or long spiral spatial periods [from 3 nm for MnGe to up to 90 nm for Fe(0.5)Co(0.5)Si] that reflect the relation between the Dzyaloshinskii-Moriya interaction and the exchange energy. In the spiral magnetic metal MnSi with $\lambda = 18$ nm, the preferred spiral directions [$1 \pm 1 \pm 1$] have the angle $\arccos(1/3) = 70.5^\circ$. If two of these directions lie in the plane of the film, the other two make the angle $\alpha = \pi/2 - \arccos(1/3) = 19.5^\circ$ with the normal OZ to the interface. In this case the structure is periodic in the OX direction with a large period $\lambda / \sin \alpha = 54$ nm, that is much larger than other characteristic lengths such as $\lambda/2\pi$ or the superconducting coherence length ξ_f . The period of the spiral in the OZ direction increases only slightly, since $\lambda / \cos \alpha = 19$ nm.

There has been some recent evidence that MnSi has a relatively weak exchange splitting [71,72]. In the compound MnSi, the amplitude of the exchange field has even been estimated [72] to take the value $h = 11$ meV, low in comparison with ferromagnetic metals. We could take the estimated value of the exchange as an upper limit for the exchange splitting of the superconducting electrons in the mean-field approximation. The exchange splitting magnitude may, however, be larger for other compounds of the B20 family. The Curie temperature may be taken as a signature of the exchange energy magnitude, though without direct proportionality. It varies from about 29 K for MnSi to 279 K for FeGe. Thus, the Curie temperature is larger than the T_c of the s -wave BCS superconducting metals like Al or Nb usually used in cryogenic nanotechnology.

As a result of the asymmetric exchange interaction, topological magnetic defects called skyrmions exist in such compounds at high magnetic fields and at temperatures close to, but below, the Curie temperature [73, 74]. These defects carry a nontrivial topological charge. Because of possible applications in spintronics [75], as well as of the fundamental interest for physical properties dictated by topology, these compounds and their films are now under very intensive theoretical and experimental investigations. Films of B20 compounds can be prepared experimentally from the single crystals by etching [76–78]. Despite their different geometry, such films have

essentially the same magnetic properties as bulk crystals. In contrast, thin films of MnSi grown by molecular beam epitaxy (MBE) or by electron-beam lithography often do not appear to host skyrmions, presumably due to their high in-plane magnetic anisotropy. In these structures, the magnetic spiral may align only with \mathbf{Q} orthogonal to the film plane. At $d_f < \lambda$ the incomplete period of the magnetic spiral may be continuously collapsed towards a uniform magnetization, replacing the conical phase in a parallel magnetic field from about a few kOe up to around 1.3 T for MnSi. This effect may also be used to tune T_c in the S/M bilayer, by gradually destroying the LRTC when approaching the situation of a uniform magnetization.

In contrast, the spiral magnetic orders in lanthanide 4f metals, such as Ho or Er, which have been widely used in experiments on the superconducting proximity effect, are characterized by short spirals, of period about 4 nm for Er and 6 nm for Ho. The order of magnitude of the exchange splitting in these materials is unsettled [79]. Furthermore, the magnetic anisotropy of such lanthanide films is usually strongly in plane.

Other model parameters. For the T_c calculations, the superconducting layer is assumed to be made of Nb, with the superconducting coherence length $\xi_s = 11$ nm. The critical temperature of the bulk superconductor is taken as $T_{cb} = 9.2$ K. The superconducting coherence length in the M layer is chosen to be $\xi_f = 4.2$ nm. The S/M interface transparency is taken from the realistic estimations made in Ref. [80] with $\gamma_B = 0.7$, and the interface parameter [48] is chosen as $\gamma = 0.7$.

III. RESULTS AND DISCUSSION

We present a systematic study of the superconducting critical temperature T_c of the S/M bilayer with a comparison for the three configurations: a spiral parallel to the S/M interface ($\cos \alpha = 0$), a spiral inclined to the interface normal by the angle $\alpha = 19.5^\circ$ (i.e., $\cos \alpha \approx 0.94$), and the case of uniform magnetization. In this last case, the superconducting properties are independent of the angle α and $Q = 0$. These three configurations allow us to compare two possible switching behaviors of the SSV, both of which may be implemented experimentally. If the S film is covered by a bulk or etched crystal of a spiral magnet of the B20 family, the change of T_c may be achieved by the switch between parallel and inclined (maybe perpendicular) spiral. Alternatively, in the case of the proximity with a M film characterized by a strong in-plane magnetic anisotropy (as in Ho, Er, or thin B20 family films), for which the spiral vector is always perpendicular to the film plane, the T_c switch may be realized by the collapse to a uniform magnetization.

In Fig. 2, the dependencies of T_c on the superconductor thickness d_s are first analyzed for different spiral configurations. Figure 2(a) shows that for a strong exchange field,

the critical temperature T_c for a parallel spiral is larger than that obtained for a uniform magnetization. This can be easily understood by the effective space averaging of the exchange field at the scale of the size of a Cooper pair. In contrast, for the inclined spiral, T_c is (slightly) reduced in comparison to the uniform case because of the draining of the Cooper pairs from the S layer into the open long-range triplet channel. This figure illustrates that the S/M proximity effect is driven by two competing mechanisms, which affect the value of T_c : (i) an effective spatial averaging of the exchange field (mostly governed by the wave vector Q of the spiral), and (ii) the appearance of the LRTC (controlled by the spiral angle and the exchange amplitude), which tends to suppress T_c .

In fact, the relative role of these two mechanisms depends on the relation between all characteristic wave vectors (including the exchange quasimomentum k_h defined from the exchange energy h , and the superconductor quasimomenta related to the coherence lengths in the S and M layers), so that the resulting behavior for T_c turns out to be a problem depending on many parameters. Our calculations reveal, as seen in Fig. 2(b), that the consideration of a smaller value for the exchange field h than taken in Fig. 2(a) can implement an opposite order for the T_c values, since the T_c for an inclined spiral is now larger than in the uniform case. It can also be seen in Fig. 2(b) that the spin-valve effect for the set of parameters related to MnSi [72] may become giant, reaching $\delta T_c \sim 1.6\text{--}1.8$ K depending on the switch to the inclined spiral or uniform magnetization. An even larger spin-valve effect is displayed in Fig. 2(d), where both a low exchange field and a short spiral period are considered. This case can motivate a direction in the search for a suitable magnetic compound with the largest possible spin-valve effect. As expected, the strongest effects resulting from the S/F interplay may be found in the regime where all characteristic length scales (the S and F superconducting coherence lengths, the spiral wavelength λ , and the magnetic length $\xi_h = k_h^{-1}$) are of the same order.

To understand the behavior according to the two mechanisms (i) and (ii) we have highlighted, it is worthwhile to recall that the long-range and short-range triplet superconducting correlations are characterized by quite different dependencies on the exchange field, which are best discriminated at strong fields: the former has a h -independent coherence length given by $(k_\omega^2 + Q^2)^{-1/2}$, while the latter can be associated with the length scale $(k_\omega^2 + k_h^2)^{-1/2}$, which is roughly inversely proportional to \sqrt{h} . The physical reason for this discrepancy is that the LRTC are not subjected to the depairing influence of the exchange field, so that both electrons in the Cooper pair can have the same spin projection to the field direction. Therefore, an increasing exchange field favors the draining of the Cooper pairs into the LRTC channel rather than into the short-range triplet channel with $S_z = 0$. At low fields, the LRTC appear

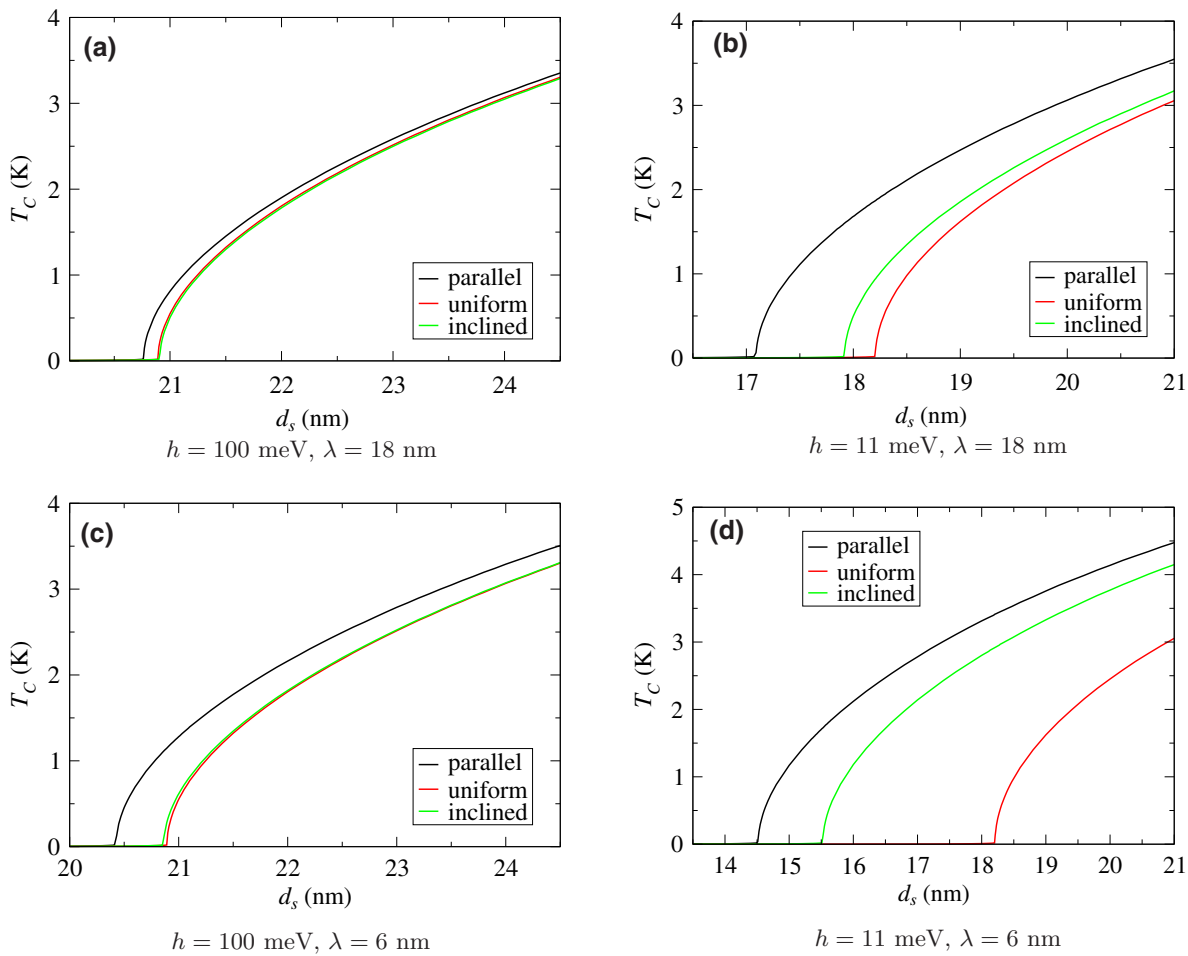


FIG. 2. Superconducting critical temperature T_c as a function of the S layer thickness d_s within three different magnetic configurations. The different panels (a)–(d) correspond to different values of the exchange energy and spiral period. The large and small exchange field cases are characterized by the typical values $h = 100$ meV and $h = 11$ meV, respectively. The long and short spiral period situations correspond to $\lambda = 18$ nm and $\lambda = 6$ nm, respectively.

as a correction in comparison with the predominantly generated short-range correlations, and thus hardly affect the superconducting properties of the M/S bilayer. In the low-exchange field regime, the T_c dependence on the spiral direction is mainly determined by the averaging mechanism: when the direction of the penetration of the Cooper pairs into the magnet is different from the direction of averaging, this averaging becomes more effective, and then T_c proved to be suppressed to a lesser extent, cf. Fig. 2(b).

Interestingly, this averaging effect on T_c may be even more pronounced in magnitude than that accompanied by the LRTC creation. It has already been noticed [81] that the scale of spatial modulation of superconducting properties in the junction plane may differ from that out of the plane. In the present study, one can also see the similarity between the integrated energetic characteristics such as T_c and the Josephson current. In the case of T_c , the out-of-plane modulation scale is weakened due to the competition with the proximity effect leakage mechanism

occurring in the same direction, so that out-of-plane modulations play quantitatively a lesser role than the in plane. If one ignores the LRTC, one can understand this effect as follows: for a perpendicular or slightly inclined spiral, the Cooper pairs encounter, when penetrating into the M layer, an almost uniform exchange field and feel its modulations weakly as they propagate. In contrast, for a magnetic spiral parallel to the interface, they experience an exchange field averaged out over the full Cooper-pair size extension.

As already remarked, the low exchange field value in the compound MnSi yields, *a priori*, a substantial spin-valve effect. As is clear from the previous discussion, another way to enhance the switching effect would be to prefer magnetic materials with strong spatial modulations, as the mean exchange averaging becomes more effective for a short spiral period. This situation is encountered, for example, in Ho with its relatively short spiral period $\lambda = 6$ nm. The corresponding T_c dependencies for the different spiral configurations are, respectively, displayed in Figs. 2(c)

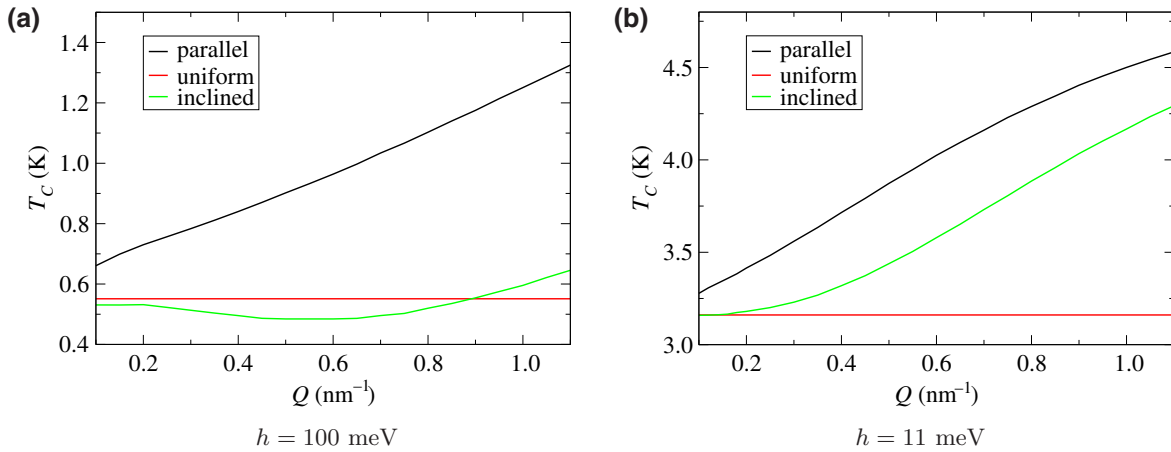


FIG. 3. Superconducting critical temperature T_c as a function of the spiral wave vector Q within three different magnetic configurations, for (a) large and (b) small exchange energy h (i.e., $h = 100$ meV and $h = 11$ meV, respectively). Here, we consider the layer thicknesses $d_f = 40$ nm and $d_s = 21$ nm.

and 2(d) for relatively large (100 meV) and small (11 meV) exchange energies [79]. From the comparison between Figs. 2(a) and 2(c) (large exchange field case), or between Figs. 2(b) and 2(d) (small exchange field case), it is clear that the averaging mechanism leads to quantitative changes in the T_c dependencies. Moreover, this effect turns out to be magnified when the magnetic length ξ_h becomes closer to the superconducting length ξ_f [a situation encountered in Figs. 2(b) and 2(d)].

From now on, we consider a S/M bilayer with a fixed S thickness ($d_s = 21$ nm; this value is chosen as more or less optimal to exhibit the dependencies) and analyze the T_c variations with respect to various other model parameters. We show in Fig. 3 that the interplay between the averaging and the LRTC mechanisms is also exhibited in the

dependence of the superconducting critical T_c on the spiral wave vector $Q = 2\pi/\lambda$. For a large exchange field, we clearly see in Fig. 3(a) an extremum in the T_c dependence of the inclined spiral. It is the result of the competition between the T_c suppression by the LRTC, which is more relevant at a long spiral, i.e., at small Q , and the effective averaging mechanism, which leads to the growth of T_c at a short spiral period, i.e., at large Q . Note that this competition does not occur in the case of a spiral parallel to the interface, for which the LRTC is absent: T_c displays a monotonic increase as a function of Q due to the more efficient averaging effect when reducing the characteristic spatial modulation of the exchange field. In contrast, at a smaller exchange field, the LRTC creation mechanism becomes less relevant, so that the extremum for the

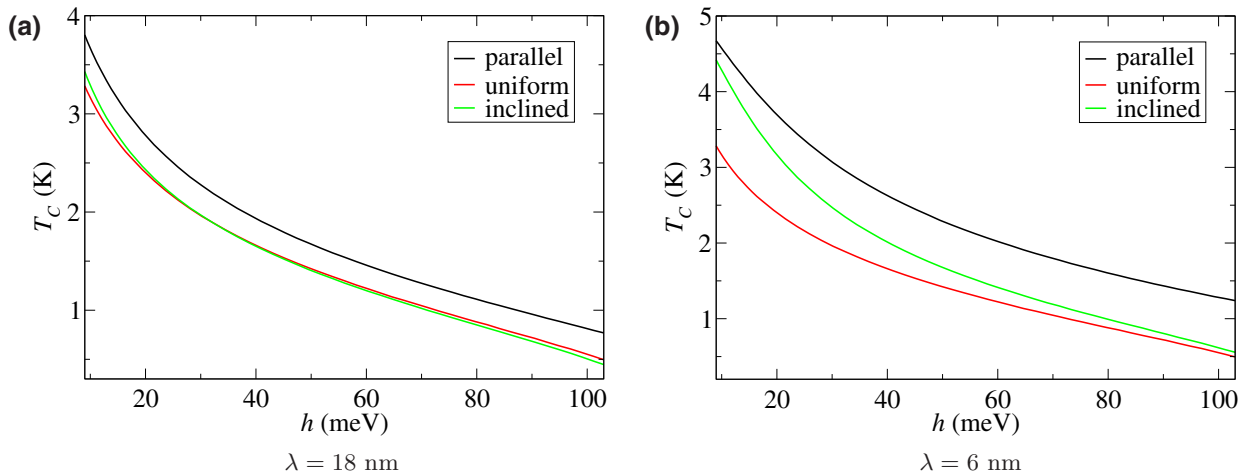


FIG. 4. Superconducting critical temperature T_c as a function of the exchange energy h within three different magnetic configurations, (a) for large spiral spatial period $\lambda = 18$ nm (as in MnSi), and (b) for short spiral spatial period $\lambda = 6$ nm (as in Ho). We take $d_s = 21$ nm and a large M -layer thickness $d_f = 40$ nm $\gg \xi_f$.

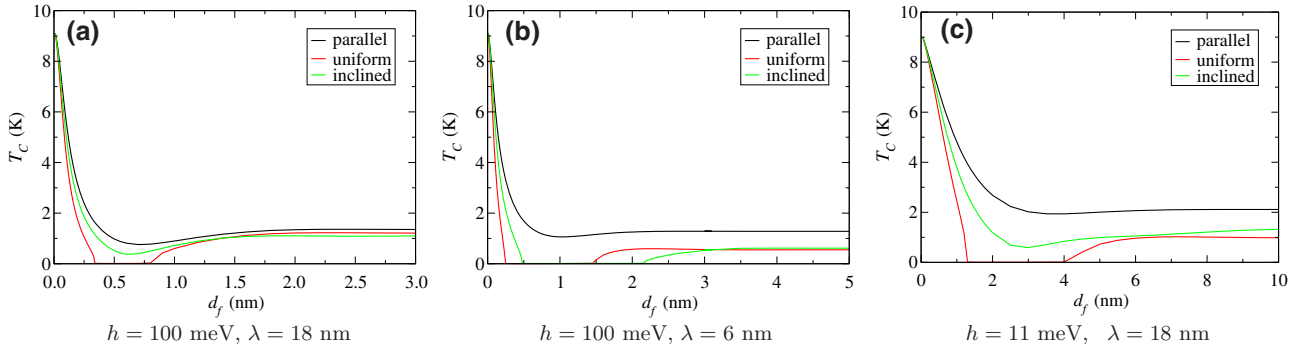


FIG. 5. Superconducting critical temperature T_c as a function of the M layer thickness d_f within three different magnetic configurations, (a) for large exchange energy $h = 100$ meV, large spiral spatial period $\lambda = 18$ nm and $d_s = 21.4$ nm, (b) large exchange energy $h = 100$ meV, short spiral spatial period $\lambda = 6$ nm and $d_s = 21$ nm, and (c) for small exchange energy $h = 11$ meV, large spiral spatial period $\lambda = 18$ nm (MnSi case).

inclined configuration shifts to much smaller values of Q as revealed in Fig. 3(b). In this situation the averaging effect dominates for most spiral periods.

To make clear the role of the exchange energy in the interplay of the two mechanisms governing the behavior of T_c that we emphasize, we present in Fig. 4(a) the dependence of T_c on h for a long spiral period (case of MnSi with $\lambda = 18$ nm). It is seen that the T_c in the different configurations display a similar (roughly parallel) decreasing tendency. In the low exchange field regime, the inclined case provides a slightly higher T_c than in the uniform case, whereas at higher exchange values it yields a lower T_c . In the inclined spiral configuration, the growth of h entails an increasing role of the LRTC in the proximity effect, which efficiently weaken the superconductivity of the S layer. At a smaller spiral period, as in Ho ($\lambda = 6$ nm), the differences in the behavior of $T_c(h)$ between the uniform and

inclined configurations is more pronounced, see Fig. 4(b). The lowest T_c is then always obtained for the uniform case.

The finite thickness of the M layer taken into account in our model calculations allows us to consider the phenomenon of reentrant superconductivity according to the spiral configuration, which is studied in some detail in Fig. 5. We point out that if one magnetic configuration provides reentrant behavior, i.e., $T_c = 0$ in some range of thickness d_f , a full switch of superconductivity may then be achieved in this range with the change of the magnetic configuration. With the decrease of the magnetic exchange energy [compare Figs. 5(a)–5(c)] the period of the T_c oscillation becomes larger, as one could expect. It thus creates better conditions for the experimental implementation of such reentrant behavior, by providing wider regions of d_f where $T_c = 0$ for a given magnetic configuration and nonzero T_c (in the Kelvin range) for another

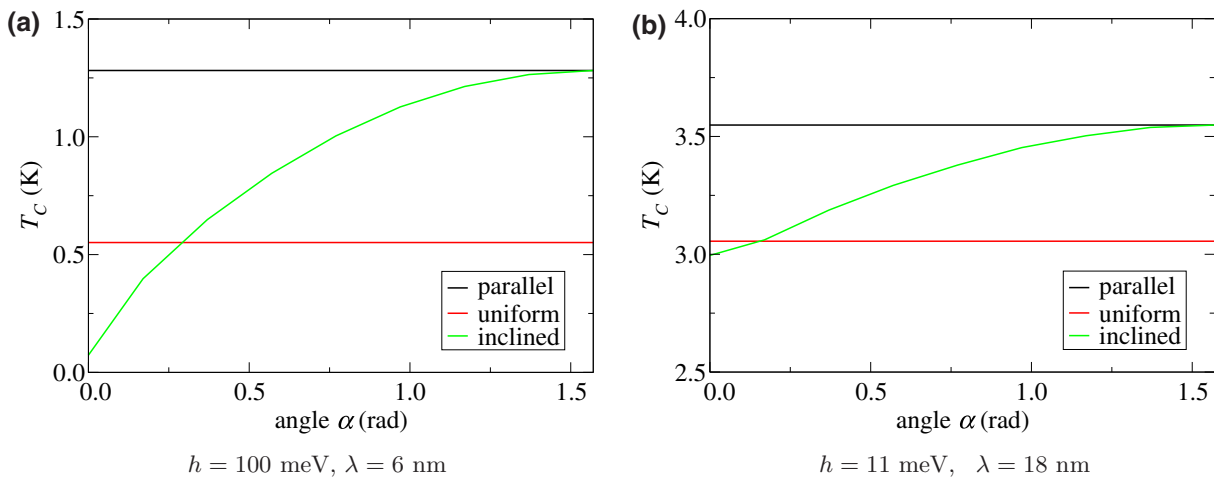


FIG. 6. Superconducting critical temperature T_c as a function of the angle α between the spiral vector Q and the S layer normal within three different magnetic configurations, (a) for large exchange $h = 100$ meV and short spiral spatial period $\lambda = 6$ nm, and (b) for small exchange $h = 11$ meV and long spiral spatial period $\lambda = 18$ nm (as in MnSi). We take equal layer thicknesses $d_s = d_f = 21$ nm. The curves in the uniform and parallel cases are kept here as reference lines.

magnetic configuration. Note that the nature of the magnetic configuration yielding a vanishing T_c in a given d_f range also depends on the magnetic exchange amplitude, in accordance with Fig. 4. For thin films grown with a strong in-plane anisotropy a possible switch may be realized by commuting the magnetic system from a spiral perpendicular to the layer to a uniform magnetization configuration. This may be achieved for a thickness smaller than the spiral period under application of a relatively small magnetic field. From this analysis, one may conclude that the compounds of the B20 family seem preferable for the observation of controlled reentrant superconductivity phenomenon and for the realization of the full switch of T_c to zero.

Finally, our model calculations also allow us to study the T_c dependence on the angle α between the spiral vector \mathbf{Q} and the S/M interface normal, see Fig. 6 with two different sets of parameters, one suitable for MnSi [Fig. 6(b)] and the other one for Ho [Fig. 6(a)]. In the two cases, the same general trend is found, namely a monotonic growth of T_c with the angle α , with an initial T_c lower than the T_c obtained in the uniform magnetization case. This stronger suppression of superconductivity for a spiral perpendicular to the film is due to the presence of the LRTC, whose generation is controlled by the angle (with a maximal production for $\alpha = 0$). The comparison between Figs. 6(a) and 6(b) shows that the LRTC plays a role at lower exchange field and at larger spiral period only within a small range of angles α for which we encounter the unusual situation where an applied magnetic field magnetizing the film uniformly may lead to an increase of the T_c of the bilayer.

IV. CONCLUSION

To summarize, we study in detail a superconducting spin valve consisting of a superconducting film covered by a spiral magnet characterized by multiple equilibrium configurations. We consider spiral magnets of different types: Ho and Er, or B20-family compounds, both crystals and films. These SSVs may be controlled by biased or pulsed external magnetic field, producing magnetization reversal or magnonic relaxation resulting in reorientation of the magnetic spiral. They present not only a fundamental theoretical interest, but also a technological one, as exemplified by the earlier experimental works [45,46] on Er or Ho bilayers and recent experimental efforts to create MnSi-based SSVs [82].

In comparison with the theoretical work developed previously in Refs. [48,59] on the same model, we present here an extended derivation including a number of significant improvements: (i) an arbitrary value of the exchange energy, suitable for MnSi for example, is considered, whereas a large value was assumed previously [48]; (ii) the magnetic spiral vector can be inclined at an

arbitrary angle with respect to the interface (for simplicity, only parallel and perpendicular spirals were considered in Ref. [48]); (iii) the finite thickness of the magnetic layer is taken into account, in contrast to the previous work [48] that assumed a semi-infinite M layer.

Besides providing a more realistic description of the possible experimental conditions and justifying some simplifications made in the previous work, this enlargement of the parameter space reveals quite different qualitative behaviors for the spin valve depending on the spiral configuration. In particular, we find that the superconducting critical temperature may significantly vary as a function of the spiral direction also at moderate or low exchange energies. In this parameter regime, the superconducting correlations resulting from the proximity effect between the superconducting film and the chiral magnet are primarily short range, so that the sensitivity of T_c is only due to the averaging of the exchange field on the scale of the Cooper pairs. It turns out that this averaging effect is much more efficient when the direction, perpendicular to the interface, of the penetration of the Cooper pairs does not coincide with the direction of the magnetic spatial inhomogeneity. As a result, the parallel spiral configuration always yields the highest T_c , as confirmed by our numerical calculations.

In contrast, for large exchange energies a different mechanism for the sensitivity of T_c is at play: for a spiral direction orthogonal to the interface the production of long-range superconducting triplet correlations opens one more channel for the leakage of the Cooper pairs from the superconducting film, thus leading to an efficient decrease of T_c . Therefore, the behavior of the studied superconducting spin valve is driven by two different antagonistic mechanisms. Our quantitative analysis of the reentrant superconductivity phenomenon in the bilayer suggests the switching behavior of the superconducting spin valve should be optimized at moderately low exchange energies, where the averaging mechanism comes to dominate that of long-range triplet correlations.

The most interesting result, which should stimulate further experimental investigation, optimization, and manufacturing of such structures, is that the spin-valve effect may yield a δT_c within the Kelvin range in MnSi-Nb bilayers, i.e., may be giant. Therefore, it seems generally preferable to manufacture SSVs with MnSi crystal-Nb bilayers. The intrinsic solution of the half-select problem and the possibility of magnonic control, that is nondestructive for the superconductivity, make such spin valves appealing for applications in cryogenic nanoelectronics.

ACKNOWLEDGMENTS

N.P. thanks D. Menzel, V. Dyadkin, and A. Bauer for helpful discussions about the B20 family properties. The

French-Russian collaboration has benefited from the Visiting Scientist Program of the Centre de Physique Théorique de Grenoble-Alpes, and from the invited researcher program of CNRS. The analysis of B20-family properties is financially supported by the Ministry of Science and Higher Education of the Russian Federation, Megagrant project N 075-15-2022-1108. N.P. thanks also the Basic Research Program and the Project Mirror Labs of the HSE University for the support of the analysis of B20-family and 4f metals-superconductor bilayers.

APPENDIX

In this Appendix, we present a detailed derivation of the key-quantity W [see Eq. (11)], which determines the dependencies of the superconducting critical temperature on the different model parameters.

For an inclined spiral, the magnetic structure is nonuniform both in OZ and OX directions, so that the different superconducting correlations components in the linearized Usadel Eq. (1) are expected to be in general functions of both x and z spatial variables, and the Laplacian operator reads $\nabla^2 = \partial^2/\partial x^2 + \partial^2/\partial z^2$.

In the orthogonal case ($\alpha = 0$), the spiral vector \mathbf{Q} lies in the OZ direction, and the magnetic field direction is described by the rotation matrix M_z around OZ axis with the rotation phase $\beta = Qz : \mathbf{h} = h(\cos\beta, \sin\beta, 0)^T = M_z(h, 0, 0)^T$. The linearized Usadel equations take the form in this case:

$$\begin{aligned} (D\nabla^2 - 2|\omega|)f_s &= 2i \operatorname{sgn}(\omega)h[f_x \cos(Qz) + f_y \sin(Qz)], \\ (D\nabla^2 - 2|\omega|)f_x &= 2i \operatorname{sgn}(\omega)hf_s \cos(Qz), \\ (D\nabla^2 - 2|\omega|)f_y &= 2i \operatorname{sgn}(\omega)hf_s \sin(Qz). \end{aligned} \quad (\text{A1})$$

From now on, we assume that the axis of the spiral is inclined in the XOZ plane. This inclined configuration may be obtained from the orthogonal case with the help of the rotation matrix around the OY axis by the angle α (OZ axis rotates towards the OX axis by the angle α)

$$M_z = \begin{pmatrix} \cos\beta & -\sin\beta & 0 \\ \sin\beta & \cos\beta & 0 \\ 0 & 0 & 1 \end{pmatrix}, \quad M_y = \begin{pmatrix} \cos\alpha & 0 & -\sin\alpha \\ 0 & 1 & 0 \\ \sin\alpha & 0 & \cos\alpha \end{pmatrix}, \quad (\text{A2})$$

where the inclined spiral vector is given by $\mathbf{Q} = M_y(0, 0, Q)^T$. The phase of the exchange field vector rotation around the spiral vector is then $\beta = \beta(x, z) = Q(-x \sin\alpha + z \cos\alpha)$. The exchange field vector reads $\mathbf{h} = M_y M_z(h, 0, 0)^T = h(\cos\alpha \cos\beta, \sin\beta, \sin\alpha \cos\beta)^T$.

The unitary transformation of the triplet components vector $\mathbf{f}_t = (f_x, f_y, f_z)^T$ to the vector $\mathbf{f} = (f_+, f_-, f_z)^T$ in the orthogonal case ($\alpha = 0$) is given by $\mathbf{f} = N\mathbf{f}_t$ with the

matrix N

$$N = \begin{pmatrix} -\exp(i\beta) & i\exp(i\beta) & 0 \\ \exp(-i\beta) & i\exp(-i\beta) & 0 \\ 0 & 0 & 1 \end{pmatrix}. \quad (\text{A3})$$

In the inclined case ($\alpha \neq 0$) all components of \mathbf{f}_t are nonzero in general. We may then introduce the vector $\mathbf{f} = (f_+, f_-, f_{zz})^T$ given by the linear transformation $\mathbf{f} = NM_y^{-1}\mathbf{f}_t$, which transforms the linearized Usadel Eq. (A1) to their linear combination. The equation for the third triplet component f_{zz} separates after the transformation and we may choose $f_{zz} = 0$, that yields the additional condition $f_z = f_x \tan\alpha$.

The explicit dependence on the x variable has completely disappeared in the equations obeyed by the correlation functions $f_{s,\pm}(x, z)$. It can be shown that the latter functions are in fact independent of x . For this purpose, we follow the method of Ref. [58] by expanding the correlations as Fourier series, assuming that the system is periodic in the OX direction: $f_{s,\pm}(x, z) \rightarrow f_{s,\pm}(m, z)$ where m is an integer number. Since the equations are linear, the different Fourier components m are fully decoupled. The most energetically favorable solution corresponds [58] to the uniform one with $m = 0$. The other solutions with $m = \pm 1, \pm 2, \dots$ describe the cases of a superconducting order parameter, which is spatially inhomogeneous even deeply in the S region and are not realized physically. Finally, we find that the functions $f_{s,\pm}(x, z)$ obey Eq. (2) in the ferromagnet, with a form similar to the orthogonal case, but with the spiral vector Q replaced by $Q \cos\alpha$ in the linear term.

The eigenvectors of the system (2) may be chosen for the eigenvalues $k_i = k_{0,\pm}$ as

$$\begin{pmatrix} u_s(k_i) \\ u_-(k_i) \\ u_+(k_i) \end{pmatrix} = \begin{pmatrix} \frac{i\frac{k_i^2-k_\omega^2}{2}+2iQk_i \cos\alpha-Q^2}{2k_h^2} \\ -\frac{\frac{k_i^2-k_\omega^2}{2}+2iQk_i \cos\alpha-Q^2}{k_i^2-k_\omega^2-2iQk_i \cos\alpha-Q^2} \\ 1 \end{pmatrix}. \quad (\text{A4})$$

For a finite F layer we also have to take into account the wave reflected from the free M -layer interface solutions which are proportional to $\exp(k_i z)$. The eigenvectors v_j representing this reflected wave may be obtained with the change $k_i \rightarrow -k_i$, considering that only the relation between the eigenvector components has a meaning

$$\begin{pmatrix} v_s(k_i) \\ v_-(k_i) \\ v_+(k_i) \end{pmatrix} = \begin{pmatrix} \frac{i\frac{k_i^2-k_\omega^2}{2}+2iQk_i \cos\alpha-Q^2}{2k_h^2} \\ -1 \\ \frac{\frac{k_i^2-k_\omega^2}{2}+2iQk_i \cos\alpha-Q^2}{k_i^2-k_\omega^2-2iQk_i \cos\alpha-Q^2} \end{pmatrix} = \begin{pmatrix} u_s(k_i) \\ -u_-(k_i) \\ -u_+(k_i) \end{pmatrix}. \quad (\text{A5})$$

Note that for $\cos \alpha = 0$ (spiral parallel to the SM interface) the two functions f_{\pm} are identical, thus indicating that only one type of triplet component (of short-range nature) is in fact produced [58] in the hybrid structure in this special configuration. In the inclined case, the system resolution necessarily involves the two different components f_+ and f_- hinting at the coexistence of two types of triplet correlations in the structure. Owing to the chirality, the short-range components (depending on the exchange field h) of the eigenvectors for the incident \mathbf{u} and reflected \mathbf{v} waves display a complicated symmetry $v_{\pm} = -u_{\mp}$, including the chirality change (“+” to “-”, and opposite). The reflected wave moves along the spiral backward and feels the opposite direction (clockwise or anticlockwise) of the magnetization rotation along the movement direction. It is worth stressing that the combination of chirality and finite thickness for the magnet leads to a computational complexity related to the doubling of the coefficient amplitudes needed, which was absent in previous publications [48,58–64].

The general form of the solution for the finite F layer is written down in Eq. (5). Let us denote $R_i \equiv A_i - B_i$ and $S_i \equiv A_i + B_i$. From the boundary conditions (8) at $z = d_f$, it follows the equations

$$\begin{aligned} \sum_i [R_i \cosh(k_i d_f) - S_i \sinh(k_i d_f)] U_{s,-}(k_i) &= 0, \\ \sum_i [S_i \cosh(k_i d_f) - R_i \sinh(k_i d_f)] U_+(k_i) &= 0, \end{aligned} \quad (\text{A6})$$

where we introduce $U_s(k_i) = u_s(k_i) k_i$ and

$$\begin{aligned} U_{\pm}(k_i) &= V_{\pm}(k_i) k_i + iQ \cos \alpha V_{\mp}(k_i). \\ V_{\pm}(k_i) &= u_+(k_i) \pm u_-(k_i). \end{aligned} \quad (\text{A7})$$

In the S layer the spatial nonuniformity is only provided by the nonuniform magnetization existing along the SM interface. It thus seems to be natural to use $\beta = \beta(x, 0)$ inside the S region. So the transformation to apply on the different superconducting components has the form $\mathbf{f}^S = N[\beta(x, 0)] M_y^{-1} \mathbf{f}_i^S$, that yields the Usadel equations in the S region

$$\begin{aligned} \left(\nabla^2 - \frac{2\omega}{D_s} \right) f_s^S &= -2\pi \frac{\Delta}{D_s}, \\ \left[\nabla^2 \pm 2iQ \sin \alpha \frac{\partial}{\partial x} - Q^2 \sin^2 \alpha - \frac{2\omega}{D_s} \right] f_{\pm}^S &= 0. \end{aligned} \quad (\text{A8})$$

As explained above, the x dependence has been dropped out in the transformed components $f_{s,\pm}$, so that we get the

equations in the S region

$$\begin{aligned} \left(\frac{\partial^2}{\partial z^2} - \frac{2\omega}{D_s} \right) f_s^S &= -2\pi \frac{\Delta}{D_s}, \\ \left[\frac{\partial^2}{\partial z^2} - Q^2 \sin^2 \alpha - \frac{2\omega}{D_s} \right] f_{\pm}^S &= 0, \end{aligned} \quad (\text{A9})$$

and $f_{zz}^S = 0$, as it is also chosen in the ferromagnet. We may search the solutions for the triplet components f_{\pm}^S satisfying the boundary condition (8) at the free interface $z = -d_s$ in the form

$$f_{\pm}^S = C_{\pm} \frac{\cosh[k_s(z + d_s)]}{\sinh(k_s d_s)}, \quad (\text{A10})$$

with the wave vector $k_s = \sqrt{Q^2 \sin^2 \alpha + 2\omega/D_s}$. The boundary conditions (9) at the SM interface ($z = 0$) read

$$\begin{aligned} \sum_i R_i V_+(k_i) + S_i U_+(k_i) \xi_f \gamma_c &= 0, \\ \sum_i S_i V_-(k_i) + R_i U_-(k_i) \xi_f \gamma_c &= 0, \end{aligned} \quad (\text{A11})$$

where $\gamma_c = \gamma_b + \gamma \coth(k_s d_s)/\xi_s k_s$. For the singlet component, we finally get the two equations:

$$\begin{aligned} \frac{\partial}{\partial z} f_s^S(0) &= -\gamma \frac{\xi_f}{\xi_s} \sum_i R_i k_i u_s(k_i), \\ f_s^S(0) &= \sum_i S_i u_s(k_i) + \gamma_b R_i k_i u_s(k_i) \xi_f. \end{aligned} \quad (\text{A12})$$

The latter equations can then be recast in the form of the reduced boundary condition (10) with the expression (11) for the value of the quantity W . The coefficients R_i, S_i are determined by using Eqs. (A6) and (A11).

-
- [1] D. S. Holmes, *et al.*, International Roadmap for devices and systems: 2018 Edition Cryogenic, Electronics and Quantum Information Processing, IEEE (2019).
 - [2] M. Eschrig, Spin-polarized supercurrents for spintronics, *Phys. Today* **64**, 43 (2011).
 - [3] J. Linder and J. W. A. Robinson, Superconducting spintronics, *Nat. Phys.* **11**, 307 (2015).
 - [4] M. G. Blamire and J. W. A. Robinson, The interface between superconductivity and magnetism: Understanding and device prospects, *J. Phys. Condens. Matter* **26**, 453201 (2014).
 - [5] M. Eschrig, Spin-polarized supercurrents for spintronics: A review of current progress, *Rep. Prog. Phys.* **78**, 104501 (2015).
 - [6] S. Oh, D. Youm, and M. R. Beasley, A superconductive magnetoresistive memory element using controlled exchange interaction, *Appl. Phys. Lett.* **71**, 2376 (1997).

- [7] A. I. Buzdin, A. V. Vedyayev, and N. V. Ryzhanova, Spin-orientation-dependent superconductivity in F/S/F structures, *Europhys. Lett.* **48**, 686 (1999).
- [8] L. R. Tagirov, Low-Field Superconducting Spin Switch Based on a Superconductor/Ferromagnet Multilayer, *Phys. Rev. Lett.* **83**, 2058 (1999).
- [9] A. Singh, S. Voltan, K. Lahabi, and J. Aarts, Colossal Proximity Effect in a Superconducting Triplet Spin Valve Based on the Half-Metallic Ferromagnet CrO₂, *Phys. Rev. X* **5**, 021019 (2015).
- [10] P. V. Leksin, N. N. Garifyanov, A. A. Kamashev, A. A. Validov, Ya. V. Fominov, J. Schumann, V. Kataev, J. Thomas, B. Büchner, and I. A. Garifullin, Isolation of proximity-induced triplet pairing channel in a superconductor/ferromagnet spin valve, *Phys. Rev. B* **93**, 100502(R) (2016).
- [11] N. O. Birge, A. E. Madden, and O. Naaman, Ferromagnetic Josephson junctions for cryogenic memory, *Proc. SPIE* **10732**, 107321M (2018).
- [12] A. Vedyayev, C. Lacroix, N. Pugach, and N. Ryzhanova, Spin-valve magnetic sandwich in a Josephson junction, *Europhys. Lett.* **71**, 679 (2005).
- [13] A. A. Golubov, M. Yu. Kupriyanov, and Ya. V. Fominov, Critical current in SFIFS junctions, *JETP Lett.* **75**, 190 (2002).
- [14] N. O. Birge, Spin-triplet supercurrents in Josephson junctions containing strong ferromagnetic materials, *Phil. Trans. R. Soc. A* **376**, 20150150 (2018).
- [15] T. I. Larkin, V. V. Bol'ginov, V. S. Stolyarov, V. V. Ryazanov, I. V. Vernik, S. K. Tolpygo, and O. A. Mukhanov, Ferromagnetic Josephson switching device with high characteristic voltage, *Appl. Phys. Lett.* **100**, 222601 (2012).
- [16] Y. V. Fominov, A. A. Golubov, and M. Y. Kupriyanov, Triplet proximity effect in FSF trilayers, *JETP Lett.* **77**, 510 (2003).
- [17] Ya. V. Fominov, A. A. Golubov, T. Y. Karminskaya, M. Yu. Kupriyanov, R. G. Deminov, and L. R. Tagirov, Superconducting triplet spin valve, *JETP Lett.* **91**, 308 (2010).
- [18] J. Y. Gu, C.-Y. You, J. S. Jiang, J. Pearson, Y. B. Bazaliy, and S. D. Bader, Magnetization-Orientation Dependence of the Superconducting Transition Temperature in the Ferromagnet-Superconductor-Ferromagnet System: CuNi/Nb/CuNi, *Phys. Rev. Lett.* **89**, 267001 (2002).
- [19] A. Potenza and C. H. Marrows, Superconductor-ferromagnet CuNi/Nb/CuNi trilayers as superconducting spin-valve core structures, *Phys. Rev. B* **71**, 180503(R) (2005).
- [20] K. Westerholt, D. Sprungmann, H. Zabel, R. Brucas, B. Hjorvarsson, D. A. Tikhonov, and I. A. Garifullin, Superconducting Spin Valve Effect of a V Layer Coupled to an Antiferromagnetic [Fe/V] Superlattice, *Phys. Rev. Lett.* **95**, 097003 (2005).
- [21] R. Steiner and P. Ziemann, Magnetic switching of the superconducting transition temperature in layered ferromagnetic/superconducting hybrids: Spin switch versus stray field effects, *Phys. Rev. B* **74**, 094504 (2006).
- [22] P. V. Leksin, A. A. Kamashev, N. N. Garifyanov, I. A. Garifullin, Ya. V. Fominov, J. Schumann, C. Hess, V. Kataev, and B. Büchner, Peculiarities of performance of the spin valve for the superconducting current, *JETP Lett.* **97**, 478 (2013).
- [23] X. L. Wang, A. Di Bernardo, N. Banerjee, A. Wells, F. S. Bergeret, M. G. Blamire, and J. W. A. Robinson, Giant triplet proximity effect in superconducting pseudo spin valves with engineered anisotropy, *Phys. Rev. B* **89**, 140508(R) (2014).
- [24] M. G. Flokstra, T. C. Cunningham, J. Kim, N. Satchell, G. Burnell, P. J. Curran, S. J. Bending, C. J. Kinane, J. F. K. Cooper, S. Langridge, A. Isidori, N. Pugach, M. Eschrig, and S. L. Lee, Controlled suppression of superconductivity by the generation of polarized Cooper pairs in spin-valve structures, *Phys. Rev. B* **91**, 060501(R) (2015).
- [25] F. S. Bergeret, A. F. Volkov, and K. B. Efetov, Josephson current in superconductor-ferromagnet structures with a nonhomogeneous magnetization, *Phys. Rev. B* **64**, 134506 (2001).
- [26] A. Kadigrobov, R. I. Shekhter, and M. Jonson, Quantum spin fluctuations as a source of long-range proximity effects in diffusive ferromagnet-superconductor structures, *Europhys. Lett.* **54**, 394 (2001).
- [27] M. Eschrig, J. Kopu, J. C. Cuevas, and Gerd Schön, Theory of Half-Metal/Superconductor Heterostructures, *Phys. Rev. Lett.* **90**, 137003 (2003).
- [28] F. S. Bergeret, A. F. Volkov, and K. B. Efetov, Odd triplet superconductivity and related phenomena in superconductor-ferromagnet structures, *Rev. Mod. Phys.* **77**, 1321 (2005).
- [29] P. V. Leksin, N. N. Garif'yanov, I. A. Garifullin, Y. V. Fominov, J. Schumann, Y. Krupskaya, V. Kataev, O. G. Schmidt, and B. Büchner, Evidence for Triplet Superconductivity in a Superconductor-Ferromagnet Spin Valve, *Phys. Rev. Lett.* **109**, 057005 (2012).
- [30] P. Leksin, N. Garif'yanov, I. Garifullin, J. Schumann, H. Vinzelberg, V. Kataev, R. Klingeler, O. G. Schmidt, and B. Büchner, Full spin switch effect for the superconducting current in a superconductor/ferromagnet thin film heterostructure, *Appl. Phys. Lett.* **97**, 102505 (2010).
- [31] B. Li, N. Roschewsky, B. A. Assaf, M. Eich, M. Epstein-Martin, D. Heiman, M. Müzenberg, and J. S. Moodera, Superconducting Spin Switch with Infinite Magnetoresistance Induced by an Internal Exchange Field, *Phys. Rev. Lett.* **110**, 097001 (2013).
- [32] Y. Gu, G. Halasz, J. Robinson, and M. Blamire, Large Superconducting Spin Valve Effect and Ultrasmall Exchange Splitting in Epitaxial Rare-Earth-Niobium Trilayers, *Phys. Rev. Lett.* **115**, 067201 (2015).
- [33] A. A. Kamashev, A. A. Validov, J. Schumann, V. Kataev, B. Büchner, Y. V. Fominov, and I. A. Garifullin, Increasing the performance of a superconducting spin valve using a Heusler alloy, *Beilstein J. Nanotechnol.* **9**, 1764 (2018).
- [34] U. D. Chacón Hernández, M. B. Fontes, E. Baggio-Saitovitch, M. A. Sousa, and C. Enderlein, Anti-Lenz supercurrents in superconducting spin valves, *Phys. Rev. B* **95**, 184509 (2017).
- [35] T. E. Baker and A. Bill, The role of canting and depleted-triplet minima in superconducting spin valve structures, *Phys. Rev. B* **97**, 214520 (2018).
- [36] E. Moen and O. T. Valls, Spin-split conductance and subgap peak in ferromagnet/superconductor spin valve heterostructures, *Phys. Rev. B* **98**, 104512 (2018).

- [37] Z. Feng, J. W. A. Robinson, and Mark Blamire, Out of plane superconducting Nb/Cu/Ni/Cu/Co triplet spin-valves, *Appl. Phys. Lett.* **111**, 042602 (2017).
- [38] D. Lenk, R. Morari, V. Zdravkov, and R. Tidecks, Full-switching FSF-type superconducting spin-triplet magnetic random access memory element, *Phys. Rev. B* **96**, 184521 (2017).
- [39] N. V. Klenov, Yu. N. Khaydukov, S. V. Bakurskiy, I. I. Soloviev, R. Morari, T. Keller, M. Yu. Kupriyanov, A. S. Sidorenko, and B. Keimer, Periodic Co/Nb pseudo spin-valve for cryogenic memory, *Beilstein J. Nanotechnol.* **10**, 833 (2019).
- [40] N. Banerjee, C. B. Smiet, R. G. J. Smits, A. Ozaeta, F. S. Bergeret, M. G. Blamire, and J. W. A. Robinson, Evidence for spin selectivity of triplet pairs in superconducting spin valves (Py-Ho-Nb-Ho-Py-FeMn), *Nat. Commun.* **5**, 3048 (2014).
- [41] I. Sosnin, H. Cho, V. T. Petrushov, and A. F. Volkov, Superconducting Phase Coherent Electron Transport in Proximity Conical Ferromagnets, *Phys. Rev. Lett.* **96**, 157002 (2006).
- [42] L. Y. Zhu, Y. Liu, F. S. Bergeret, J. E. Pearson, S. G. E. te Velthuis, S. D. Bader, and J. S. Jiang, Unanticipated Proximity Behavior in Ferromagnet-Superconductor Heterostructures with Controlled Magnetic Noncollinearity, *Phys. Rev. Lett.* **110**, 177001 (2013).
- [43] F. Chiodi, J. D. S. Witt, R. G. J. Smits, L. Qu, G. B. Halász, C.-T. Wu, O. T. Valls, K. Halterman, J. W. A. Robinson, and M. G. Blamire, Supra-oscillatory critical temperature dependence of Nb-Ho bilayers, *Europhys. Lett.* **101**, 37002 (2013).
- [44] Y. Gu, G. B. Halász, J. W. A. Robinson, and M. G. Blamire, Large Superconducting Spin Valve Effect and Ultrasmall Exchange Splitting in Epitaxial Rare-Earth-Niobium Trilayers, *Phys. Rev. Lett.* **115**, 067201 (2015).
- [45] A. Di Bernardo, S. Diesch, Y. Gu, J. Linder, G. Divitini, C. Ducati, E. Scheer, M. G. Blamire, and J. W. A. Robinson, Signature of magnetic-dependent gapless odd frequency states at superconductor/ferromagnet interfaces, *Nat. Commun.* **6**, 8053 (2015).
- [46] N. Satchell, J. D. S. Witt, M. G. Flokstra, S. L. Lee, J. F. K. Cooper, C. J. Kinane, S. Langridge, and G. Burnell, Control of Superconductivity with a Single Ferromagnetic Layer in Niobium/Erbium Bilayers, *Phys. Rev. Appl.* **7**, 044031 (2017).
- [47] I. V. Vernik, V. V. Bol'ginov, S. V. Bakurskiy, A. A. Golubov, M. Yu. Kupriyanov, V. V. Ryazanov, and O. A. Mukhanov, Magnetic Josephson junctions with superconducting interlayer for cryogenic memory, *IEEE Trans. Appl. Supercond.* **23**, 1701208 (2013).
- [48] N. G. Pugach, M. Safonchik, T. Champel, M. E. Zhito-mirsky, E. Lahderanta, M. Eschrig, and C. Lacroix, Superconducting spin valves controlled by spiral re-orientation in B20-family magnets, *Appl. Phys. Lett.* **111**, 162601 (2017).
- [49] N. A. Gusev, D. I. Dgheparov, N. G. Pugach, and V. I. Belotelov, Magnonic control of the superconducting spin valve by magnetization reorientation in a helimagnet, *Appl. Phys. Lett.* **118**, 232601 (2021).
- [50] Y. Ishikawa, G. Shirane, J. A. Tarvin, and M. Kohgi, Magnetic excitations in the weak itinerant ferromagnet MnSi, *Phys. Rev. B* **16**, 4956 (1977).
- [51] C. Pfleiderer, S. R. Julian, and G. G. Lonzarich, Non-Fermi-liquid nature of the normal state of itinerant-electron ferromagnets, *Nature* **414**, 427 (2001).
- [52] M. Uchida, Y. Onose, Y. Matsui, and Y. Tokura, Real-space observation of helical spin order, *Science* **311**, 359 (2006).
- [53] S. V. Grigoriev, S. V. Maleyev, V. A. Dyadkin, D. Menzel, J. Schoenes, and H. Eckerlebe, Principal interactions in the magnetic system $\text{Fe}_{1-x}\text{Co}_x\text{Si}$: Magnetic structure and critical temperature by neutron diffraction and SQUID measurements, *Phys. Rev. B* **76**, 092407 (2007).
- [54] V. Dyadkin, S. V. Grigoriev, D. Menzel, D. Chernyshov, V. Dmitriev, J. Schoenes, S. V. Maleyev, E. V. Moskvin, and H. Eckerlebe, Control of chirality of transition-metal monosilicides by the Czochralski method, *Phys. Rev. B* **84**, 014435 (2011).
- [55] S. Mühlbauer, B. Binz, F. Jonietz, C. Pfleiderer, A. Rosch, A. Neubauer, R. Georgii, and P. Böni, Skyrmion lattice in a chiral magnet, *Science* **323**, 915 (2009).
- [56] A. Fert, V. Cros, and J. Sampaio, Skyrmions on the track, *Nat. Nanotech.* **8**, 152 (2013).
- [57] D. Menzel, D. Schroeter, N. Steinki, S. Süllow, A. Fernández Scarioni, H. W. Schumacher, H. Okuyama, H. Hidaka, and H. Amitsuka, Hall effect and resistivity in epitaxial MnSi thin films under ambient and high pressure, *IEEE Trans. Magn.* **55**, 1500204 (2019).
- [58] T. Champel and M. Eschrig, Switching superconductivity in superconductor/ferromagnet bilayers by multiple-domain structures, *Phys. Rev. B* **71**, 220506(R) (2005).
- [59] A. F. Volkov, A. Anishchanka, and K. B. Efetov, Odd triplet superconductivity in a superconductor/ferromagnet system with a spiral magnetic structure, *Phys. Rev. B* **73**, 104412 (2006).
- [60] G. B. Halász, J. W. A. Robinson, J. F. Annett, and M. G. Blamire, Critical current of a Josephson junction containing a conical magnet, *Phys. Rev. B* **79**, 224505 (2009).
- [61] G. B. Halász, M. G. Blamire, and J. W. A. Robinson, Magnetic-coupling-dependent spin-triplet supercurrents in helimagnet/ferromagnet Josephson junctions, *Phys. Rev. B* **84**, 024517 (2011).
- [62] C.-T. Wu, O. T. Valls, and K. Halterman, Proximity effects in conical-ferromagnet/superconductor bilayers, *Phys. Rev. B* **86**, 184517 (2012).
- [63] K. Halterman and M. Alidoust, Half-metallic superconducting triplet spin valve, *Phys. Rev. B* **94**, 064503 (2016).
- [64] A. A. Jara, C. Safranski, I. N. Krivorotov, C.-T. Wu, A. N. Malmi-Kakkada, O. T. Valls, and K. Halterman, Angular dependence of superconductivity in superconductor/spin-valve heterostructures, *Phys. Rev. B* **89**, 184502 (2014).
- [65] Note that for itinerant electrons a similar magnetic texture appears in a metal with intrinsic spin-orbit interaction [83,84]. By finding a way to control intrinsic spin-orbit interaction one may be able to explore such a spin-valve structure like a Josephson junction with a two-dimensional electron gas.
- [66] T. Champel and M. Eschrig, Effect of an inhomogeneous exchange field on the proximity effect in disordered superconductor-ferromagnet hybrid structures, *Phys. Rev. B* **72**, 054523 (2005).

- [67] T. Champel, T. Löfwander, and M. Eschrig, $0 - \pi$ Transitions in a Superconductor/Chiral Ferromagnet/Superconductor Junction Induced by a Homogeneous Cycloidal Spiral, *Phys. Rev. Lett.* **100**, 077003 (2008).
- [68] M. Yu. Kuprianov and V. F. Lukichev, Influence of boundary transparency on the critical current of “dirty” SS’S structures, *Zh. Eksp. Teor. Fiz.* **94**, 139 (1988). [Sov. Phys. JETP **67**, 1163 (1988)].
- [69] Ya. V. Fominov, N. M. Chtchelkatchev, and A. A. Golubov, Nonmonotonic critical temperature in superconductor/ferromagnet bilayers, *Phys. Rev. B* **66**, 014507 (2002).
- [70] T. Löfwander, T. Champel, and M. Eschrig, Phase diagrams of ferromagnet-superconductor multilayers with misaligned exchange fields, *Phys. Rev. B* **75**, 014512 (2007).
- [71] M. Janoschek, M. Garst, A. Bauer, P. Krautscheid, R. Georgii, P. Boni, and C. Pfleiderer, Fluctuation-induced first-order phase transition in Dzyaloshinskii-Moriya helimagnets, *Phys. Rev. B* **87**, 134407 (2013).
- [72] A. Bauer, talk at DPG Spring Meeting, Berlin, March 11–16, (2018).
- [73] A. Neubauer, C. Pfleiderer, B. Binz, A. Rosch, R. Ritz, P. G. Niklowitz, and P. Böni, Topological Hall Effect in the A Phase of MnSi, *Phys. Rev. Lett.* **102**, 186602 (2009).
- [74] Y. Li, N. Kanazawa, X. Z. Yu, A. Tsukazaki, M. Kawasaki, M. Ichikawa, X. F. Jin, F. Kagawa, and Y. Tokura, Robust Formation of Skyrmions and Topological Hall Effect Anomaly in Epitaxial Thin Films of MnSi, *Phys. Rev. Lett.* **110**, 117202 (2013).
- [75] T. L. Monchesky, Skyrmions: Detection with unpolarized currents, *Nat. Nanotech.* **10**, 1008 (2015).
- [76] A. Tonomura, X. Z. Yu, K. Yanagisawa, T. Matsuda, Y. Onose, N. Kanazawa, H. S. Park, and Y. Tokura, Real-space observation of skyrmion lattice in helimagnet MnSi thin samples, *Nano Lett.* **12**, 1673 (2012).
- [77] M. Mochizuki, X. Z. Yu, S. Seki, N. Kanazawa, W. Koshiba, J. Zang, M. Mostovoy, Y. Tokura, and N. Nagaosa, Thermally driven ratchet motion of a skyrmion microcrystal and topological magnon Hall effect, *Nat. Mater.* **13**, 241 (2014).
- [78] X. Yu, A. Kikkawa, D. Morikawa, K. Shibata, Y. Tokunaga, Y. Taguchi, and Y. Tokura, Variation of skyrmion forms and their stability in MnSi thin plates, *Phys. Rev. B* **91**, 054411 (2015).
- [79] Different papers [32,43,46,60] have reported very different estimations for the exchange energy splitting in rare-earth metals such as Ho or Er. The splittings are usually inferred from a fit to specific theoretical models, which do not always take into account all the possible mechanisms of the proximity effect in these materials: LTC creation, space averaging, and spiral magnetic structure. In contrast, the exchange energy values extracted from micromagnetic or first-principles calculations relate more to localized spins, and thus may serve only as an upper limit for the exchange splitting in the conducting band, which contributes to superconducting pairing. Consequently, in the present theoretical description we cover all cases from small to large exchange to show the ways of optimizing SSVs once these parameters are known.
- [80] N. G. Pugach, M. Yu. Kupriyanov, E. Goldobin, R. Kleiner, and D. Koelle, Superconductor-insulator-ferromagnet-superconductor Josephson junction: From the dirty to the clean limit, *Phys. Rev. B* **84**, 144513 (2011).
- [81] N. G. Pugach, M. Yu. Kupriyanov, A. V. Vedyayev, C. Lacroix, E. Goldobin, D. Koelle, R. Kleiner, and A. S. Sidorenko, Ferromagnetic Josephson junctions with step-like interface transparency, *Phys. Rev. B* **80**, 134516 (2009).
- [82] J. Grefe, *Proximity-Effekte in Nb-B20-Heterostrukturen*, Bachelor thesis, Braunschweig Technical University, (2018).
- [83] I. V. Bobkova, A. M. Bobkov, and M. A. Silaev, Generalized quasiclassical theory of the long-range proximity effect and spontaneous currents in superconducting heterostructures with strong ferromagnets, *Phys. Rev. B* **96**, 094506 (2017).
- [84] F. S. Bergeret and I. V. Tokatly, Spin-orbit coupling as a source of long-range triplet proximity effect in superconductor-ferromagnet hybrid structures, *Phys. Rev. B* **89**, 134517 (2014).